Pseudorotation barriers of biological oxyphosphoranes: a challenge for simulations of ribozyme catalysis

Carlos Silva Lopez[1,2], Olalla Nieto Faza[1],
Angel Rodriguez de Lera[1] and Darrin M. York[3,*]

1. Departamento de Quimica Organica, Universidade de Vigo, Lagoas Marcosende, 36200, Vigo, Galicia, Spain

2. Kimika Fakultatea, P.K. 1072, 20080 Donostia, Euskadi, Spain.

3. Department of Chemistry, University of Minnesota, 207 Pleasant St. SE, Minneapolis, MN 55455–0431, USA.

[*] *Correspondence: york@chem.umn.edu*

Abstract

Pseudorotation reactions of biologically relevant oxyphosphoranes were studied using density-functional and continuum solvation methods. A series of 16 pseudorotation reactions involving acyclic and cyclic oxyphosphoranes in neutral and monoanionic (singly deprotonated) forms were studied, in addition to pseudorotation of PF_5. The effect of solvent was treated using 3 different solvation models for comparison. The barriers to pseudorotation ranged from 1.5 to 8.1 kcal/mol and were influenced systematically by charge state, apicophilicity of ligands, intramolecular hydrogen bonding, cyclic structure and solvation. Barriers to pseudorotation for monoanionic phosphoranes occur with the anionic oxo ligand as the pivotal atom, and are generally lower than for neutral phosphoranes. The OCH_3 groups were observed to be more apicophilic than OH groups, and hence pseudorotations that involve axial OCH_3/equatorial OH exchange had higher reaction and activation free energy values. Solvent generally lowered barriers relative to the gas phase reactions. These results, together with isotope ^{18}O exchange experiments, support the assertion that dianionic phosphoranes are not sufficiently long-lived to undergo pseudorotation. Comparison of the density-functional results with those from several semiempirical quantum models highlight a challenge for new-generation hybrid quantum mechanical/molecular mechanical potentials for non-enzymatic and enzymatic phosphoryl transfer reactions: the reliable modeling of pseudorotation processes.

1 Introduction

The chemistry of biological phosphate systems is seamlessly linked to life supporting processes such as the regulation of blood pH, energy transfer, cell signaling and recognition,[1] and RNA catalysis.[2] Of particular interest are the molecular mechanisms of phosphoryl transfer reactions catalyzed by enzymes and ribozymes.[3,4] In order to provide insight into these mechanisms, a tremendous amount of experimental and theoretical work has focused on the characterization of key factors that influence the reactivity of biological phosphates and quantification of the energy barriers associated with transition states and reactive intermediates along the pathways that lead to different products.[5–8] An understanding of these factors provides insight into biological activity and may assist in the design of new pharmaceutical compounds or biotechnology.

A common mechanism for the transesterification or hydrolysis reactions of biological phosphates involves an in-line nucleophilic attack to a phosphate center that results in the displacement of a leaving group. The intermediates and/or transition states for this type of reaction are pentavalent phosphorane species. According to the rules of Westheimer,[9] bond formation and cleavage are likely to occur only in the axial position of the phosphorane. The lifetime of the phosphorane intermediate depends upon the nature of the phosphorane (i.e., the ligands around the phosphorus center), its charge (protonation) state, and its interaction with solvent, metal ions and functional groups that occur in a macromolecular (e.g., enzyme) environment. If a phosphorane intermediate is sufficiently long-lived, it may undergo a process of pseudorotation that alters the stereochemistry and/or the distribution of reaction products. Consequently, it is of considerable interest to characterize the barriers of pseudorotation for different biologically relevant oxyphosphoranes.

The Berry pseudorotation process[10] involves an interconversion of a pentacoordinate trigonal bipyramidal species whereby there is an exchange of two ligands in the axial positions with two ligands in the equatorial positions (Scheme 1). The process can be visualized as a conformational re-arrangement that involves two concerted bending motions (a contraction and a widening of the angle between exchanging axial and equatorial ligands, respectively) with one of the equatorial ligands (the "pivotal" atom) held fixed. After a square pyramidal transition state, the system regains bipyramidal structure resulting in an apparent rotation (pseudorotation) of the original trigonal bipyramid structure.

Theoretical electronic structure methods, and in particular hybrid density-functional theory (DFT) methods, have been extensively applied to pentavalent phosphoranes and shown to be considerably reliable. Some recent applications include analysis of anharmonic frequencies[11] and pseudorotation[12] of PF_5, the calculation of phosphorane pK_as,[13] and phosphate hydrolysis reactions.[14] Very recently, hybrid DFT has been applied to the study of biological metaphosphate, phosphate and phosphorane compounds,[15] including binding of divalent Mg^{2+} ions,[16] and pseudorotation barriers of chemically modified phosphoranes.[17]

The present work is focused on the characterization of key factors that influence the rate of pseudorotation of biologically relevant oxyphosphoranes including: 1) protonation state, 2) degree of esterification, 3) acyclic and cyclic ligand structure and 4) solvation. Density-functional calculations are performed on a series of 16 pseudorotation reactions of oxyphosphoranes, and also for the pseudorotation of PF_5 as a baseline comparison. The effect of solvation is considered with three different implicit solvation models. The DFT results are compared with those of several semiempir-

ical Hamiltonian models that are routinely used in hybrid quantum mechanical/molecular mechanical (QM/MM) simulations of phosphoryl transfer reactions in aqueous[18,19] and enzymatic environments[14] in order to identify potential problem areas for these methods when modeling biological reactions. The DFT results presented here can be used toward the design of new semiempirical quantum models that more accurately represent the potential energy surface for phosphoryl transfer reactions.

2 Methods

2.1 Density-functional Calculations

Electronic structure calculations for the biological oxyphosphoranes presented in this work (Table 1) were performed using Kohn-Sham density functional theory (DFT) with the hybrid exchange functional of Becke[20,21] and the Lee, Yang, and Parr correlation functional[22] (B3LYP). Energy minimum and transition state geometry optimizations were performed in redundant internal coordinates with default convergence criteria,[23] and stability conditions of the restricted closed shell Kohn-Sham determinant for each final structure were verified.[24,25] Frequency calculations were performed to establish the nature of all stationary points and to allow evaluation of thermodynamic quantities.

The geometry optimization and frequency calculations were performed using the 6–31++G(d,p) basis set. Electronic energies and other properties of the density were further refined via single point calculations at the optimized geometries using the 6–311++G(3df,2p) basis set and the B3LYP hybrid density functional. The basis sets used for geometry optimization and frequency calculations in the present work are slightly larger than the corresponding basis sets used in the G2[26,27] and G3[28,29] methods, and similar to the basis sets used in the G3X[30] method that typically yield

atomization energies within 1 kcal/mol or less of experimental values. Single point calculations were run with convergence criteria on the density matrix tightened to 10^{-8} *au* on the SCF wave function to ensure high precision for properties sensitive to the use of diffuse basis functions.[31] This protocol applied to obtain the (refined energy)//(geometry and frequencies) is designated by the abbreviated notation B3LYP/6–311++G(3df,2p)//B3LYP/6–31++G(d,p). All density-functional calculations were performed with the GAUSSIAN03[32] suite of programs (with the exception of the SM5 solvation calculations, see below). Thermodynamic properties at 298.15 K were obtained from the density-functional calculations using standard statistical mechanical expressions for separable vibrational, rotational and translational contributions within the harmonic oscillator, rigid rotor, ideal gas/particle-in-a-box models in the canonical ensemble,[33] and have been described in detail elsewhere.[15] The standard state in the gas phase is for a mole of particles at $T = 298.15$ K and 1 atm pressure.

2.2 Solvation Models

Solvent effects were taken into account with sequential single point calculations at the gas phase-optimized B3LYP/6–31++G(d,p) geometries as in previous work.[15,17] Three different solvation models[34] were considered for comparison: 1) the polarizable continuum model (PCM),[35–37] 2) a variation of the conductor-like screening model (COSMO)[38] (employing the parameters provided by Klamt and coworkers[39]) as implemented in Gaussian03,[32,40] and 3) the SM5.42R solvation model (SM5)[41] as implemented in MN-GSM.[42]

The solvation free energy, ΔG_{sol}, is defined as

$$\Delta G_{sol} = G_{aq} - G_{gas} \tag{1}$$

where G_{gas} and G_{aq} are the molecular free energies in the gas phase and in aqueous solution, respectively. In the present work the approximation is made that the gas-phase geometry, entropy and thermal corrections to the enthalpy do not change upon solvation. This approximation is consistent with that of recent work on related systems[15–17] where the protocol was tested against the most relevant available experimental values and found to be reliable for the models considered. The practical reason for introducing this approximation resides in the difficulty and computational cost associated with the calculation of stationary points and Hessians with the boundary element solvation methods.

Within these approximations, the solvation energy is given by

$$\Delta G_{sol} = \left(E\left[\Psi_{sol}\right] + E_{sol}\left[\rho_{sol}\right]\right) - E\left[\Psi_{gas}\right] \tag{2}$$

where $E\left[\Psi_{gas}\right]$ and $E\left[\Psi_{sol}\right]$ are the the Kohn-Sham energy functionals that take as arguments the Kohn-Sham single-determinant wave function optimized in the gas phase (Ψ_{gas}) and in solution (Ψ_{sol}), and $E_{sol}\left[\rho_{sol}\right]$ is the solvation energy that takes as argument the polarized electron density in solution ρ_{sol} (which can be derived from Ψ_{sol}).

All PCM and COSMO calculations were performed at the B3LYP/6–311++G(3df,2p)//B3LYP/6–31++G(d,p) level as for the gas phase calculations using the UAKS radii.[43] All SM5.42R calculations were carried out using the B3LYP functional and the MIDI! basis set[44] at the optimized gas-phase geometries. The SM5.42R/B3LYP/MIDI! model was parameterized using HF/MIDI! derived geometries; however, the original SM5.42R model does not appear to be overly sensitive to small changes in geometry.[41] Additional details on the application of this method to related systems is discussed elsewhere.[15]

3 Results and Discussion

This section presents results and discussion of density-functional calculations on biologically important oxyphosphorane pseudorotation reactions. The first subsection introduces an abbreviated nomenclature convention to facilitate further presentation and discussion. The following subsections are organized into topical areas that involve: geometrical structure, kinetic barriers and reaction thermodynamics, and solvation effects, respectively.

3.1 Nomenclature

Scheme 1 illustrates the structure and general symbolic nomenclature for acyclic and cyclic phosphorane minima and pseudorotation transition states. The series of phosphorane minima with their abbreviated symbolic nomenclature definitions are listed in Table 1. The phosphorane ligands, arranged in order of increasing complexity, are generically labeled “A” and “B” in the axial positions, and “R”, “S”, and “E” in the equatorial positions (Scheme 1). This nomenclature is consistent with that of previous work on biological metaphosphate, phosphate and phosphorane compounds.[15] A minimum energy phosphorane structure is designated in the general expanded notation as P(R)(S)(E)(A)(B), as shown under the column heading *Molecule* in Table 1. Since cyclic phosphoranes having a 5-membered ring must have one end of the ring in the equatorial position and one in the axial position,[9] the notation can also be made to accommodate this situation as P(R)(S)(-EA-)(B). The nomenclature convention described only leaves unattended the fact that enantiomers may occur. In the present work, enantiomers are not enumerated, and geometric quantities are reported in such a way as to avoid the need for stereochemical distinction.

In order to avoid propagating the rather cumbersome expanded phosphorane notation "P(R)(S)(E)(A)(B)" throughout the manuscript, the following abbreviated symbolic notation is introduced (Table 1):

$$P_{A/C}^{(Rn)} - \#^{charge}$$

where P stands for phosphorous, Rn is the Roman numeral that gives the coordination number for the phosphorous (always "V" in the present work, but can vary as in previous work),[15] A/C stands for "acyclic"/"cyclic", respectively, and # is an alpha-numeric index assigned to each of the trigonal bipyramidal phosphorane minimum structures in Table 1. Phosphoranes with different chemical formulas have different leading integers in their alpha-numeric index. If there are two conformers with the same chemical formula, the designations "a" or "b" are appended to the leading integer to form the alpha-numeric index in order of increasing gas-phase free energy ("a" has a lower gas-phase free energy than "b"). For the sake of clarity structures have been arranged in Table 1 so that the numeric value in # coincides with the number of hydroxy ligands in the neutral molecule. Abbreviations for monoanionic (i.e., singly deprotonated) phosphoranes are based on the neutral phosphorane abbreviation and indicated by a minus superscript.

Pseudorotation reactions and corresponding rate-controlling transition states are designated by bracketing the alpha-numeric index of the related minima. In the Berry pseudorotation process[10] one ligand (the "pivotal" group) remains immobile while the other two pairs of ligands interchange their respective axial and equatorial positions (Scheme 1). For reactions, the pivotal ligand is indicated by boldface type in Table 1. Unless otherwise explicitly stated, all deprotonation occurs at the pivotal atom position in the pseudorotation reaction since a pseudorotation that involves an oxyanion in the axial position is considerably unfavorable. This situation will be revisited as a special case at the

end of the subsection 3.3.

3.2 Structure

3.2.1 Minimum Energy Structures

The structures of the oxyphosphoranes corresponding to the local minimum energy initial and final states of pseudorotation have predominantly trigonal bipyramidal character (Table 2). The pattern of bond lengths and deviation from ideal trigonal bipyramidal structure (i.e., θ_1=180° and θ_2=120°, Scheme 1), can be traced back to the charge state of the system and/or the cyclic or acyclic character of the substituents. Thus, the following general trends can be derived.

For *oxyphosphorane bond lengths*:

- axial (P–O_{ax}) bond lengths *are greater than* equatorial (P–O_{eq}) bond lengths
- for monoanionic phosphoranes, axial and equatorial (P–O_{ax} and P–O_{eq}) bond lengths to neutral ligands *are greater than* the corresponding bond lengths in the neutral phosphoranes due, in part, to larger repulsions arising from the anionic oxo ligand
- for monoanionic phosphoranes, the anionic P–O^-_{eq} bond length *is shorter than* all other equatorial bond lengths due to partial double bond character that develops to delocalize the formal negative charge
- for a given charge state, axial P–O_{ax}(C) bonds *are longer than* the corresponding P–O_{ax}(H) bonds
- for cyclic phosphoranes, endocyclic P–O_{ax}(C) bond lengths *are greater than* exocyclic P–O_{ax}(C) bond lengths (about 0.05 Å), in agreement with previous theoretical work[15] and with the experimental enhanced susceptibility to hydrolysis of cyclic versus acyclic phosphates[5](although the role of solvation is important[45]).
- for acyclic phosphoranes, P–O_{ax}(H) and P–O_{eq}(H) bond lengths *are slightly greater than* the corresponding bond lengths of cyclic phosphoranes

and for *oxyphosphorane bond angles*:

- for neutral phosphoranes, O_{ax}–P–O_{ax}, O_{ax}–P–O_{eq} and O_{eq}–P–O_{eq} bond angles *are close to* the ideal values of 180, 90 and 120 degrees, respectively while the increased repulsion of the pivotal anionic oxo ligand in monoanionic phosphoranes distorts their structures from these values
- for monoanionic phosphoranes, O_{ax}–P–O_{ax}, O_{ax}–P–O_{eq} and O_{eq}–P–O_{eq} bond angles *are smaller than* those of corresponding neutral phosphoranes

- for monoanionic phosphoranes, O_{eq}–P–O^{-}_{eq} and O_{ax}–P–O^{-}_{eq} bond angles *are larger than* those of corresponding neutral phosphoranes
- for acyclic and cyclic phosphoranes in the same charge state, corresponding O–P–O bond angles *are very similar*; i.e., O–P–O bond angles are largely unaffected by acyclic versus cyclic structure

3.2.2 Transition State Structures

Mean structural parameters for the rate-controlling pseudorotation transition states for the oxyphosphoranes are summarized in Table 3. Also included for comparison is a well-studied benchmark model phosphorane, PF_5. For the purposes of discussion a parameter to measure the square pyramid character of the transition states has been defined as %SP $= [1 - |\theta_1 - \theta_2|/60] \times 100$. For the prototypical PF_5, which exhibits an ideal square pyramidal pseudorotation transition state, the %SP value is then 100% (Scheme 1), this parameter would be 0 for an ideal bipyramid. The %SP parameter correlates well with other parameters, such as bond lengths, used to characterize the transition states. For the neutral systems, the mean axial and equatorial bond lengths are in general more similar to one another for the transition state structures that have greater square pyramidal character; i.e., $< bl_{ax} > \approx < bl_{eq} >$ for %SP $\approx$ 100. The largest difference between $< bl_{ax} >$ and $< bl_{eq} >$ for neutral phosphorane transition states is 0.021 Å for $P_A^{(V)}-[\mathbf{4a, 4b}]$ that has the least square pyramidal character (%SP=92.2).

The monoanionic structures exhibit a greater degree of structural diversity. For two of the monoanionic acyclic molecules, the pseudorotation proceeds through a symmetric, square-pyramidal transition state ($P_A^{(V)}-[\mathbf{1, 1}]^-$ and $P_A^{(V)}-[\mathbf{5, 5}]^-$), similar to those found for the neutral phosphoranes, with only moderate deviations. These structures display slightly bigger distortions in bond lengths and smaller overall θ_1 and θ_2 angles with %SP values of 100. The differences between these

monoanionic phosphorane transition states and those of the corresponding neutral phosphoranes arise from the greater repulsion of the pivotal atom in the former, which holds localized negative charge. The other monoanionic acyclic pseudorotation reactions proceed through distorted transition states with considerably less square pyramidal character (%SP values ranging between 38.5 and 93.5). For these systems the change in the average bond lengths in the reactants and transition structures is also considerably larger and the differences $\theta_1 - \theta_2$ range from 15 to 30 degrees.

The largest change (contraction) in axial bond lenghts is observed in the monoanionic cyclic phosphorane transition states, due in part to the fact these bond lengths are particularly long in the corresponding minima. The longer bond lengths of the cyclic structures are due in part to ring strain, and related to the experimentally observed enhanced reactivity of cyclic phosphates.[6] Pseudorotation of the monoanionic phosphoranes tend to exhibit early or late transition states that influence the pseudorotation barriers in accord with the Hammond postulate[46] (see below).

3.3 Kinetic Barriers and Reaction Thermodynamics

The kinetic and thermodynamic characterization of pseudorotation reactions of oxyphosphoranes is important for the understanding of non-enzymatic and enzymatic phosphoryl transfer reactions. If a phosphorane generated in a hydrolysis or transesterification reaction is sufficiently long-lived, it may undergo pseudorotation, altering the stereochemical outcome of the reaction or leading to different products such as those of phosphate migration[5–7] (Scheme 2). The key kinetic and thermodynamic quantities for the pseudorotation process of the present work are listed in Table 4, where the direction of the reactions is chosen so that the ΔG values are greater than or equal to zero.

Three main factors govern the kinetics and thermodynamics of the gas-phase reactions: 1) the

apicophilicity of the substituents, 2) the protonation state of the phosphoranes and 3) the changes in intramolecular hydrogen bonding. The profiles for acyclic and cyclic, neutral and monoanionic pseudorotation reactions are illustrated as a function of the reaction coordinate $(\theta_1 - \theta_2)/60$ in Fig. 1.

From the ΔG values for the endothermic reactions, it is evident that an OH group is considerably less apicophilic than an OCH_3 group,[15,47] since all the entries with $\Delta H > 0$ and $\Delta G > 0$ involve one or more OCH_3 groups in the axial position interchanging with OH in the equatorial position. These results are consistent with other work on biological phosphorus compounds.[15]

As a result, processes that involve the greater number of exchanges of equatorial OH groups with axial OCH_3 groups generally have higher reaction enthalpies and free energies that serve to raise the kinetic barriers of the forward reaction in accord with the Hammond postulate.[46] For example, the acyclic/cyclic and neutral/monoanionic pseudorotation reactions ($P_A^{(V)}-[\mathbf{3a},\mathbf{3b}]$, $P_A^{(V)}-[\mathbf{3a},\mathbf{3b}]^-$, $P_C^{(V)}-[\mathbf{3},\mathbf{3}]$ and $P_C^{(V)}-[\mathbf{3},\mathbf{3}]^-$) that involve no net OH/OCH_3 exchanges all have lower reaction free energies and activation barriers than the corresponding reactions that involve a single net OH/OCH_3 exchange ($P_A^{(V)}-[\mathbf{2a},\mathbf{2b}]$, $P_A^{(V)}-[\mathbf{2a},\mathbf{2b}]^-$, $P_C^{(V)}-[\mathbf{2a},\mathbf{2b}]$ and $P_C^{(V)}-[\mathbf{2a},\mathbf{2b}]^-$, respectively).

As discussed in section 3.2, monoanionic phosphoranes present considerable geometric distortions compared with the more symmetric neutral phosphoranes. Distortion of the monoanionic phosphoranes from a trigonal bipyramidal structure toward that of a transition state-like square pyramid is one of the key factors that result in the general lowering of the monoanionic pseudorotation transition state barriers. The range of activation barriers for the monoanionic phosphoranes (1.5-7.7 kcal/mol) is considerably larger than for the neutral phosphoranes (5.4-8.1 kcal/mol). The lower

barriers observed for anionic systems that have the negatively charged pivotal oxygen can be readily explained by the increased axial-equatorial repulsions that arise from the shorter P-O bond length and the delocalized negative charge of this ligand. These repulsions lead to distorted minima (e.g., with axial angles typically bent by around 14°) that are closer both in structure and in energy to the square pyramidal transition states.

For most pseudorotation reactions in the present work, the change in the number of intramolecular hydrogen bonds that occurs in going from the reactant to the product (Δn_{HB}) is 0 and in going from reactant to the transition state ($\Delta n^{\ddagger}_{HB}$) is 0 or -1 (Table 4). In general, pseudorotations of neutral phosphoranes where a single hydrogen bond is broken during the reaction ($\Delta n^{\ddagger}_{HB}$=-1, corresponding $\Delta G^{\ddagger}$ values range from 7.0-8.1 kcal/mol) have transition state structures that are moderately more destabilized than those where no disruption is observed ($\Delta n^{\ddagger}_{HB}$=-0, corresponding $\Delta G^{\ddagger}$ values range from 5.4-6.3 kcal/mol). Hence, an estimate for the destabilization energy due to intramolecular hydrogen bond disruption for neutral phosphorane pseudorotation reaction ranges between 0.7-2.7 kcal/mol per hydrogen bond with a mean value of approximately 1.7 kcal/mol. The anionic phosphorane pseudorotation reactions exhibit a higher degree of variation with respect to changes in intramolecular hydrogen bonding. This large variation stems from the more diverse hydrogen bonding environment in the anionic phosphoranes. Relatively weak intramolecular hydrogen bonds can form between neutral ligands (OH→OH and OH→OCH_3), or stronger intramolecular hydrogen bonds can occur between a neutral and an anionic ligand (OH→O^-). As mentioned previously, the repulsive interactions of the negative oxo ligand in the anionic phosphoranes also have a large effect on the activation barriers that is only mildly correlated with $\Delta n^{\ddagger}_{HB}$. Together, these

competing factors tend to obscure the general trends in the activation barriers for the anionic pseudorotation reactions compared with the neutral pseudorotation reactions.

Pseudorotation of an oxyanion to the axial position. In order to quantify the generally accepted assertion that the pseudorotation process for anionic phosphoranes proceed with the anionic oxo ligand as the pivotal atom, the pseudorotation of $P_A^{(V)}-\mathbf{5}^-$ was considered where the oxo ligand is a basal atom in the reactant and occupies an axial position in the product (i.e., one of the equatorial OH ligand was taken as the pivotal atom).

The structure of this transition state exhibits a shorter average equatorial bond lengths (1.639 Å opposed to 1.739 Å in $P_A^{(V)}-[\mathbf{5},\mathbf{5}]^-$) due mainly to the shorter P–O$^-$bond that has moderate double bond character in order to delocalize the negative charge. The angles at the transition state, θ_1 = 163.7 and θ_2 = 147.0 lead to a %SP value of 72.2%. The product of this pseudorotation process exhibits a structure with a mean O$^-$–P–OH angle of 94.3° and the three equatorial OH ligands forming hydrogen bonds with the axial anionic oxo group. (Fig. 2).

The reaction free energy and activation barrier for the pseudorotation of the anionic oxo ligand from the equatorial position to the axial position are 9.68 and 11.75 kcal/mol, respectively. These values are considerably higher than the corresponding values (0.0 and 7.19 kcal/mol, respectively) for the alternate pseudorotation path that proceeds through the $P_A^{(V)}-[\mathbf{5},\mathbf{5}]^-$ transition state. Consequently, it is unlikely that at physiological temperatures the pseudorotation that positions the anionic oxo ligand axially would be kinetically or thermodynamically significant. The transition state and the product of this pseudorotation bear resemblance in both geometric and energetic features, in accord with the Hammond postulate.[46] This behavior can be readily understood from a simple

VSEPR model: anionic substituents have greater repulsion and prefer to occupy equatorial positions to alleviate the strain with other electron pairs at (roughly) 90° associated with an apical position. These results are consistent with previous calculations that indicate that anionic axial phosphorane ligands are considerably less stable than the neutral ones.[15]

3.4 Solvation Effects

Solvation provides tremendous stabilization of phosphate and phosphorane anions,[15] influences the conformational flexibility of phosphate esters[48] and has a profound effect on the free energy profile for hydrolysis reactions.[45,49] Pseudorotation reactions of model phosphate systems, such as methyl ethylene phosphate, connect reaction paths that lead to products of endocyclic and exocyclic cleavage.[5,6] In fact, it has been proposed that in the hydrolysis of methyl ethylene phosphate under alkaline conditions, the attack of a hydroxyl group is concerted with pseudorotation.[50] Despite numerous studies on the effect of solvation on phosphate hydrolysis in-line attack mechanisms[45,51–56] and associative and dissociative pathways,[49,57–59] considerably less attention has been paid to the more subtle influence of solvation on pseudorotation reactions of biological phosphoranes.[17] This topic is addressed in the present section.

Solvation effects were treated using the PCM,[35] COSMO[38] and SM5[34] solvation models (see Methods). Table 5 compares values for the change in solvation free energy for the net reaction ($\Delta\Delta G_{sol}$) and for the rate-controlling transition state ($\Delta\Delta G^{\ddagger}_{sol}$) calculated with each of the solvation models. The non-zero $\Delta\Delta G_{sol}$ values are generally in reasonable agreement between the PCM and COSMO methods (these methods are similar in that they are both types of boundary element methods that use a common set of parameterized radii), the largest variation being 0.5 kcal/mol

for $P_A^{(V)}-[\mathbf{2a},\mathbf{2b}]$ and $P_C^{(V)}-[\mathbf{1a},\mathbf{1b}]$. The SM5 $\Delta\Delta G_{sol}$ values differ slightly from the corresponding PCM and COSMO values, the former being generally smaller in magnitude, and in three instances ($P_A^{(V)}-[\mathbf{3a},\mathbf{3b}]$, $P_A^{(V)}-[\mathbf{4a},\mathbf{4b}]$ and $P_A^{(V)}-[\mathbf{1a},\mathbf{1b}]^-$) differ in sign.

Overall, the $\Delta\Delta G_{sol}$ values tend to be negative and fairly small, the most negative values being -2.45, -2.58 and -1.79 kcal/mol for PCM, COSMO and SM5, respectively. Phosphoranes with OCH_3/OH occupying the equatorial/axial positions tend to have more favorable solvation energy values relative to the axial/equatorial isomers. For neutral phosphoranes, the $\Delta\Delta G_{sol}$ values tend to become less favorable with increasing number of OH groups, whereas the opposite trend occurs for the monoanionic phosphoranes. Given that the gas-phase ΔG values are positive or zero (by convention), the negative $\Delta\Delta G_{sol}$ values increase the equilibrium constant for the reactions in solution relative to that in the gas phase, but (with two exceptions, see below) are not sufficient in magnitude to result in an exergonic reaction.

The solvent stabilization of the transition states are indicated by the $\Delta\Delta G^{\ddagger}_{sol}$ values in Table 5. Overall, the correspondence between the PCM, COSMO and SM5 values for $\Delta\Delta G^{\ddagger}_{sol}$ is closer than for the $\Delta\Delta G_{sol}$ values (due in part to the fact that the geometric changes are smaller in going from reactant to transition state as opposed to going from reactants to products). As expected, the reference system ($P_F^{(V)}-\mathbf{1}$) is not strongly affected by the presence of solvent, the estimated magnitude of the $\Delta\Delta G^{\ddagger}_{sol}$ values all falling below 0.1 kcal/mol. As with the values for $\Delta\Delta G_{sol}$ in Table 5, the $\Delta\Delta G^{\ddagger}_{sol}$ values are predominantly negative, and lower the free energy of activation for pseudorotation in solution relative to the gas phase. With the exception of $P_A^{(V)}-[\mathbf{1},\mathbf{1}]^-$ and $P_C^{(V)}-[\mathbf{1a},\mathbf{1b}]^-$ that have positive $\Delta\Delta G^{\ddagger}_{sol}$ values, the solvent stabilization of the transition states relative to the reactants

is generally larger for the monoanionic phosphoranes. The monoanionic phosphoranes for which $\Delta\Delta G^{\ddagger}_{sol}$ is the least favorable involve transition states where the intramolecular hydrogen bonding arrangement is preserved (i.e., $\Delta n^{\ddagger}_{HB}$=0: $P_A^{(V)}-[\mathbf{1},\mathbf{1}]^-$, $P_C^{(V)}-[\mathbf{1a},\mathbf{1b}]^-$ and $P_A^{(V)}-[\mathbf{3a},\mathbf{3b}]^-$).

The calculated total reaction and activation free energy values are listed in Table 6. Only in the case of the PCM and COSMO calculations for $P_A^{(V)}-[\mathbf{3a},\mathbf{3b}]$ and $P_C^{(V)}-[\mathbf{1a},\mathbf{1b}]^-$ does the inclusion of solvent change the sign of the net reaction free energy. The activation barriers in solution are considerably lower than in the gas phase. For the most part, the general conclusions regarding the trends in activation barriers observed in the gas phase are maintained. Of particular significance are the observations that:

- pseudorotation barriers for oxyphosphoranes in solution *are fairly low*, ranging from about 1.5-7.5 kcal/mol
- pseudorotation barriers for monoanionic phosphoranes *are lower than* for neutral phosphoranes
- pseudorotation barriers for cyclic phosphoranes *are slightly lower than* for corresponding acyclic phosphoranes

As an example, for the PCM solvation model, the activation barriers for neutral acyclic and cyclic oxyphosphoranes range from 5.53-7.20 and 5.03-6.27 kcal/mol, respectively, and for monoanionic acyclic and cyclic oxyphosphoranes range from 3.44-4.35 and 1.60-2.64 kcal/mol, respectively. Similar trends are evident from the COSMO and SM5 solvation models, although the ranges of activation barriers are somewhat larger for the SM5 solvation model.

An important consequence of this work involves the interpretation of kinetic data for the hydrolysis of phosphates in solution that serve as model systems to characterize the factors that govern biological phosphate reactivity. For example, the hydrolysis of methyl ethylene phosphate (MEP), first discussed by Westheimer,[9] is described schematically as involving fast pseudorotation under

acidic conditions where the phosphorane intermediate is neutral, and slow pseudorotation under mildly alkaline conditions where the phosphorane is monoanionic.[5] The present calculations suggest that pseudorotation of the phosphorane intermediate in the hydrolysis of MEP (Figure 3) is not a result of the barriers to pseudorotation being increased for the monoanionic cyclic oxyphosphorane relative to the neutral one. Instead, it is more likely that pseudorotation occurs more readily under acidic conditions due to a prolonged lifetime of the neutral phosphorane intermediate.

Pseudorotation in ethylene phosphate can be measured experimentally by the uptake of ^{18}O from isotopically labeled water molecules[5] (Scheme 3). In order for ^{18}O to be incorporated, an isotopically labeled water makes an in-line nucleophilic attack to the phosphate to form an oxyphosphorane intermediate. The reaction can either proceed to the endocyclic cleavage product, or revert back to the reactants via exocyclic cleavage of the nucleophile-phosphate bond. Alternately, if the lifetime of the phosphorane intermediate is sufficiently long for pseudorotation to occur, subsequent exocyclic cleavage results in ^{18}O incorporation to form isotopically labeled ethylene phosphate. It has been observed experimentally that incorporation of ^{18}O in ethylene phosphate occurs only under non-alkaline conditions.[5] The results of the present work suggest that pseudorotation of the monoanionic phosphorane is not rate-limiting since the barrier for this process is only around 1.6 kcal/mol in solution (Table 6). This supports the hypothesis[5] that the observed ^{18}O exchange is due to the fact that, under sufficiently alkaline conditions, the dianionic phosphorane is a transition state, or else a kinetically insignificant intermediate,[6] that is not sufficiently long lived to undergo protonation by solvent and subsequent pseudorotation. The results presented here are consistent with calculations on pseudorotation of chemically modified cyclic biological phosphoranes.[17]

3.5 Semiempirical Calculations

The resolution of atomic-level details and quantitative assessment of reaction barriers for catalytic RNA processes remains a challenge for theoretical methods. Simulations of reactions in non-enzymatic and enzymatic environments using hybrid QM/MM calculations[60–62] afford a particularly promising strategy for inclusion of the complex characteristics of condensed-phase environment and sampling of the many degrees of freedom. These methods, however, require very fast quantum methods in order to be feasible. The most commonly applied class of quantum methods in QM/MM calculations are self-consistent semiempirical Hamiltonian models. These methods have been recently applied to study transphosphorylation thio effects of a 3' ribose-phosphate model system in solution.[18,19]

Conventional semiempirical Hamiltonian models are limited in their accuracy in simulations[61,62] and linear-scaling calculations[63,64] of enzyme or ribozyme reactions. Due to the importance of these applications, the field continues to work toward improvement of these models,[65–67] especially for thermochemistry and kinetics. It has been well established that two major problem areas involve the development of methods that can accurately predict barriers to reactions that involve chemical bond formation and cleavage, and that accurately reproduce correct relative conformational energies and barriers. The former problem can be partially alleviated with careful re-parameterization of the models so as to include data for reaction barriers.[67] A more satisfactory solution to both of these problems involves re-design of the semiempirical model itself to include features such as "orthogonalization corrections"[68] and other terms that correct systematic problems.[65,66] A recent, but related, alternative to these semiempirical models is a self-consistent density-functional method[69] that ap-

pears to be very promising and has been successfully applied to some biological reactions.[70,71]

The data presented in the current work represents an important set of benchmarks for new quantum models designed to model phosphoryl transfer reactions. Pseudorotation of biological phosphoranes involve a concerted conformational transition of a hypervalent phosphorus that may be further complicated by anionic character and intramolecular hydrogen bonding interactions. These factors combine to make accurate semiempirical modeling of pseudorotation reactions particularly challenging.

Table 7 compares ΔH and $\Delta H^{\ddagger}$ values for pseudorotation processes computed with several established semiempirical Hamiltonians (see Section 2) with those of the present work. It is evident from Table 7 that the all of the semiempirical methods perform poorly for these processes. Different Hamiltonians offer not only quantitatively different values, but also qualitatively different results: sometimes predicting reaction enthalpies of the wrong sign, barrierless transitions, or else finding minima where there should be a transition state. Generally, the differences between the semiempirical and DFT results exceed the 50% of the actual ΔH obtained with DFT calculations. A general trend is that the semiempirical methods underestimate the pseudorotation activation barriers, and also predict 5-membered ring structures that are not properly puckered (e.g., are predicted to be too planar). These problems are likely inherent to the NDDO approximation, whereby the overlap matrix is treated as the unit matrix, that affects two-center exchange interactions. These problem might be overcome in new-generation semiempirical models that properly include this type of exchange effect.[68,69] The MNDO/d method gives the best overall description of phosphorane structure, with the exception that it does not predict intramolecular hydrogen bonding. For pseudorotation reactions,

however, there remains room for considerable improvement.

4 Conclusion

The present work describes results of hybrid density-functional calculations of oxyphosphorane pseudorotations. The results provide quantitative insight into the factors that influence the structure, free energies and activation barriers of these processes, and have implications into related steps in non-enzymatic and enzymatic phosphoryl transfer reactions that involve phosphorane intermediates.

Hydroxy ligands were observed to be less apicophilic than methoxy groups. Pseudorotation reactions for neutral and monoanionic phosphoranes were fairly low, ranging from 1.5 to 8.1 kcal/mol. Barriers to pseudorotation for monoanionic phosphoranes occur with the anionic oxo ligand as the pivotal atom, and were generally lower than for neutral phosphoranes. The lowering of the monoanionic pseudorotation barriers results from distortion of the phosphorane by repulsions of the pivotal anionic oxo ligand to form a more transition state-like square pyramidal structure.

These results, together with isotope ^{18}O exchange experiments, support the assertion that dianionic phosphoranes are not sufficiently long-lived to undergo pseudorotation.[5] Cyclic phosphoranes undergo pseudorotation slightly more readily than do acyclic phosphoranes with the same number of carbon atoms. Solvation generally has a preferential stabilization effect on the transition states that tends to lower the pseudorotation barriers relative to the gas phase values.

Results of conventional semiempirical calculations for pseudorotation processes are shown not to be reliable. These results highlight a new challenge for the new-generation semiempirical quantum models for phosphoryl transfer reactions: the accurate modeling of pseudorotation processes. The results presented here provide insight into the factors that influence the pseudorotation rates of

biological phosphoranes and serve as benchmark data for the design of new quantum models for non-enzymatic and enzymatic phosphoryl transfer.

5 Acknowledgment

DY is grateful for financial support provided by the National Institutes of Health (Grant 1R01-GM62248-01A1), and the Army High Performance Computing Research Center (AHPCRC) under the auspices of the Department of the Army, Army Research Laboratory (ARL) under Cooperative Agreement number DAAD19-01-2-0014. Computational resources were provided by the Minnesota Supercomputing Institute. CS and NF are grateful for FPU fellowships provided by the Spanish Ministerio de Educacion y Ciencia.

References

(1) AHN, N. Introduction: Protein Phosphorylation and Signaling. *Chem. Rev.* **101**, 8 (2001), 2207–2208.

(2) SCOTT, W. G. RNA catalysis. *Curr. Opin. Struct. Biol.* **8**, 6 (1998), 720–726.

(3) SCOTT, W. G. Biophysical and biochemical investigations of RNA catalysis in the hammerhead ribozyme. *Q. Rev. Biophys.* **32** (1999), 241–294.

(4) DOHERTY, E. A., AND DOUDNA, J. A. Ribozyme Structures and Mechanisms. *Annu. Rev. Biophys. Biomol. Struct.* **30** (2001), 457–475.

(5) PERREAULT, D. M., AND ANSLYN, E. V. Unifying the Current Data on the Mechanism of Cleavage-Transesterification of RNA. *Angew. Chem. Int. Ed.* **36** (1997), 432–450.

(6) ZHOU, D.-M., AND TAIRA, K. The Hydrolysis of RNA: From Theoretical Calculations to the Hammerhead Ribozyme-Mediated Cleavage of RNA. *Chem. Rev.* **98** (1998), 991–1026.

(7) OIVANEN, M., KUUSELA, S., AND LÖNNBERG, H. Kinetics and Mechanisms for the Cleavage and Isomerization of the Phosphodiester Bonds of RNA by Brnsted Acids and Bases. *Chem. Rev.* **98** (1998), 961–990.

(8) HENGGE, A. C. Isotope effects in the study of phosphoryl and sulfuryl transfer reactions. *Acc. Chem. Res.* **35** (2002), 105–112.

(9) WESTHEIMER, F. H. Pseudo-rotation of the hydrolysis of phosphate esters. *Acc. Chem. Res.* **1** (1968), 70–78.

(10) STEPHEN, B. R. Correlation of rates of intramolecular tunneling processes, with application to some Group V compounds. *J. Chem. Phys.* **32** (1960), 933–938.

(11) CALIGIANA, A., AQUILANTI, V., BURCL, R., HANDY, N. C., AND TEW, D. P. Anharmonic frequencies and Berry pseudorotation motion in PF5. *Chem. Phys. Lett.* **369** (2003), 335–344.

(12) DAUL, C., FRIOUD, M., SCHAFER, O., AND SELLONI, A. Non-empirical dynamical DFT calculation of the Berry pseudorotation of PF5. *Chem. Phys. Lett.* **262** (1996), 74–79.

(13) LOPEZ, X., SCHAEFER, M., DEJAEGERE, A., AND KARPLUS, M. Theoretical evaluation of pK_a in phosphoranes: implications for phosphate ester hydrolysis. *J. Am. Chem. Soc.* **124**, 18 (2002), 5010–5018.

(14) LOPEZ, X., YORK, D. M., DEJAEGERE, A., AND KARPLUS, M. Theoretical Studies on the Hydrolysis of Phosphate Diesters in the Gas Phase, Solution, and RNase A. *Int. J. Quantum Chem.* **86** (2002), 10–26.

(15) RANGE, K., MCGRATH, M. J., LOPEZ, X., AND YORK, D. M. The Structure and Stability of Biological Metaphosphate, Phosphate, and Phosphorane Compounds in the Gas Phase and in Solution. *J. Am. Chem. Soc.* **126** (2004), 1654–1665.

(16) MAYAAN, E., RANGE, K., AND YORK, D. M. Structure and binding of Mg(II) ions and di-metal bridge complexes with biological phosphates and phosphoranes. *J. Biol. Inorg. Chem., in press*, 2004.

(17) LÓPEZ, C. S., FAZA, O. N., GREGERSEN, B. A., LOPEZ, X., DE LERA, A. R., AND YORK, D. M. Pseudorotation of Natural and Chemically Modified Biological Phosphoranes: Implications for RNA Catalysis. *Chem. Phys. Chem.* **5** (2004), 1045–1049.

(18) GREGERSEN, B. A., LOPEZ, X., AND YORK, D. M. Hybrid QM/MM study of thio effects in transphosphorylation reactions. *J. Am. Chem. Soc.* **125** (2003), 7178–7179.

(19) GREGERSEN, B. A., LOPEZ, X., AND YORK, D. M. Hybrid QM/MM Study of Thio Effects in Transphosphorylation Reactions: The Role of Solvation. *J. Am. Chem. Soc.* **126** (2004), 7504–7513.

(20) BECKE, A. D. Density-functional exchange-energy approximation with correct asymptotic behavior. *Phys. Rev. A.* **38** (1988), 3098–3100.

(21) BECKE, A. D. Density-functional thermochemistry. iii. the role of exact exchange. *J. Chem. Phys.* **98**, 7 (1993), 5648–5652.

(22) LEE, C., YANG, W., AND PARR, R. G. Development of the Colle-Savetti Correlation energy formula into a funcional of the electron density. *Phys. Rev. B.* **37** (1988), 785–789.

(23) PENG, C., AYALA, P. Y., SCHLEGEL, H. B., AND FRISCH, M. J. Using redundant internal coordinates to optimize equilibrium geometries and transition states. *J. Comput. Chem.* **17** (1996), 49–56.

(24) BAUERNSCHMITT, R., AND AHLRICHS, R. Stability analysis for solutions of the closed shell Kohn Sham equation. *J. Chem. Phys.* **104** (1996), 9047–9052.

(25) SEEGER, R., AND POPLE, J. A. Self-consistent molecular orbital methods. XVIII. Constraints and stability in Hartree?Fock theory. *J. Chem. Phys.* **66**, 7 (1977), 3045–3050.

(26) CURTISS, L. A., JONES, C., TRUCKS, G. W., RAGHAVACHARI, K., AND POPLE, J. A. Gaussian-1 theory of molecular energies for second-row compounds. *J. Chem. Phys.* **93**, 4 (1990), 2537–2545.

(27) CURTISS, L. A., CARPENTER, J. E., RAGHAVACHARI, K., AND POPLE, J. A. Validity of additivity approximations used in GAUSSIAN-2 theory. *J. Chem. Phys.* **96**, 12 (1992), 9030–9034.

(28) CURTISS, L. A., REDFERN, P. C., RAGHAVACHARI, K., RASSOLOV, V., AND POPLE, J. A. Gaussian-3 theory using reduced Møller-Plesset order. *J. Chem. Phys.* **110** (1999), 4703–4709.

(29) CURTISS, L. A., RAGHAVACHARI, K., REDFERN, P. C., AND POPLE, J. A. Assessment of Gaussian-3 and density functional theories for a larger experimental test set. *J. Chem. Phys.* **112** (2000), 7374–7383.

(30) CURTISS, L. A., REDFERN, P. C., RAGHAVACHARI, K., AND POPLE, J. A. Gaussian-3X (G3X) theory: Use of improved geometries, zero-point energies, and Hartree-Fock basis sets. *J. Chem. Phys.* **114**, 1 (2001), 108–117.

(31) ÆLEEN FRISCH, AND MICHAEL J. FRISCH. *Gaussian 98 User's Reference*, 2nd ed. Gaussian, Inc., Pittsburgh, PA, 1999.

(32) FRISCH, M. J., TRUCKS, G. W., SCHLEGEL, H. B., SCUSERIA, G. E., ROBB, M. A., CHEESEMAN, J. R., MONTGOMERY JR., J. A., VREVEN, T., KUDIN, K. N., BURANT, J. C., MILLAM, J. M., IYENGAR, S. S., TOMASI, J., BARONE, V., MENNUCCI, B., COSSI, M., SCALMANI, G., REGA, N., PETERSSON, G. A., NAKATSUJI, H., HADA, M., EHARA, M., TOYOTA, K., FUKUDA, R., HASEGAWA, J., ISHIDA, M., NAKAJIMA, T., HONDA, Y., KITAO, O., NAKAI, H., KLENE, M., LI, X., KNOX, J. E., HRATCHIAN, H. P., CROSS, J. B., ADAMO, C., JARAMILLO, J., GOMPERTS, R., STRATMANN, R. E., YAZYEV, O., AUSTIN, A. J., CAMMI, R., POMELLI, C., OCHTERSKI, J. W., AYALA, P. Y., MOROKUMA, K., VOTH, G. A., SALVADOR, P., DANNENBERG, J. J., ZAKRZEWSKI, V. G., DAPPRICH, S., DANIELS, A. D., STRAIN, M. C., FARKAS, O., MALICK, D. K., RABUCK, A. D., RAGHAVACHARI, K., FORESMAN, J. B., ORTIZ, J. V., CUI, Q., BABOUL, A. G., CLIFFORD, S., CIOSLOWSKI, J., STEFANOV, B. B., LIU, G., LIASHENKO, A., PISKORZ, P., KOMAROMI, I., MARTIN, R. L., FOX, D. J., KEITH, T., AL-LAHAM, M. A., PENG, C. Y., NANAYAKKARA, A., CHALLACOMBE, M., GILL, P. M. W., JOHNSON, B., CHEN, W., WONG, M. W., GONZALEZ, C., AND POPLE, J. A. Gaussian 03, Revision B.01. Gaussian, Inc., Pittsburgh PA, 2003.

(33) CRAMER, C. J. *Essentials of Computational Chemistry: Theories and Models*. John Wiley & Sons, Chichester, England, 2002.

(34) CRAMER, C. J., AND TRUHLAR, D. G. Implicit solvation models: equilibria, structure, spectra, and dynamics. *Chem. Rev.* **99**, 8 (1999), 2161–2200.

(35) TOMASI, J., AND PERSICO, M. Molecular interaction in solution: An overview of methods based on continuous distributions of the solvent. *Chem. Rev.* **94** (1994), 2027–2094.

(36) MINEVA, T., RUSSO, N., AND SICILIA, E. Solvation Effects on Reaction Profiles by the Polarizable Continuum Model Coupled with the Gaussian Density Functional Method. *J. Comput. Chem.* **19**, 3 (1998), 290–299.

(37) COSSI, M., SCALMANI, G., REGA, N., AND BARONE, V. New developments in the polarizable continuum model for quantum mechanical and classical calculations on molecules in solution. *J. Chem. Phys.* **117** (2002), 43–54.

(38) KLAMT, A., AND SCHÜÜRMANN, G. COSMO: a new approach to dielectric screening in solvents with explicit expressions for the screening energy and its gradient. *J. Chem. Soc. Perkin Trans. 2* **2** (1993), 799–805.

(39) KLAMT, A., JONAS, V., BÜRGER, T., AND LOHRENZ, J. C. W. Refinement and Parametrization of COSMO-RS. *J. Phys. Chem. A* **102** (1998), 5074–5085.

(40) BARONE, V., AND COSSI, M. Quantum Calculation of Molecular Energies and Energy Gradients in Solution by a Conductor Solvent Model. *J. Phys. Chem. A* **102** (1998), 1995–2001.

(41) LI, J., ZHU, T., HAWKINS, G. D., WINGET, P., LIOTARD, D. A., CRAMER, C. J., AND TRUHLAR, D. G. Extension of the platform of applicability of the SM5.42R universal solvation model. *Theor. Chem. Acc.* **103** (1999), 9–63.

(42) XIDOS, J. D., LI, J., THOMPSON, J. D., HAWKINS, G. D., WINGET, P. D., ZHU, T., RINALDI, D., LIOTARD, D. A., CRAMER, C. J., TRUHLAR, D. G., AND FRISCH, M. J. MN-GSM,version 1.8. University of Minnesota, Minneapolis, MN 55455-0431, 2001.

(43) BARONE, V., COSSI, M., AND TOMASI, J. A new definition of cavities for the computation of solvation free energies by the polarizable contiuum model. *J. Chem. Phys.* **107**, 8 (1997), 3210–3221.

(44) EASTON, R. E., GIESEN, D. J., WELCH, A., CRAMER, C. J., AND TRUHLAR, D. G. The MIDI! basis set for quantum mechanical calculations of molecular geometries and partial charges. *Theor. Chem. Acc.* **93**, 5 (1996), 281–301.

(45) DEJAEGERE, A., LIM, C., AND KARPLUS, M. Dianionic Pentacoordinate Species in the Base-Catalyzed Hydrolysis of Ethylene and Dimethyl Phosphate. *J. Am. Chem. Soc.* **113** (1991), 4353–4355.

(46) HAMMOND, G. S. A Correlation of Reaction Rates. *J. Am. Chem. Soc.* **77** (1955), 334–338.

(47) HOLMES, R. R. A model for calculating conformational energies in pentacoordinate phosphorus compounds. *J. Am. Chem. Soc.* **100**, 2 (1978), 433–446.

(48) FLORIÁN, J., ŠTRAJBL, M., AND WARSHEL, A. Conformational flexibility of phosphate, phosphonate, and phosphorothioate methyl esters in aqueous solution. *J. Am. Chem. Soc.* **120** (1998), 7959–7966.

(49) FLORIÁN, J., AND WARSHEL, A. Phosphate ester Hydrolysis in aqueous solution: Associative versus dissociative mechanisms. *J. Phys. Chem. B* **102** (1998), 719–734.

(50) LIM, C., AND TOLE, P. Concerted Hydroxyl Ion Attack and Pseudorotation in the Base-Catalyzed Hydrolysis of Methyl Ethylen Phosphate. *J. Phys. Chem.* **96** (1992), 5217–5219.

(51) DEJAEGERE, A., AND KARPLUS, M. Hydrolysis Rate Difference between Cyclic and Acyclic Phosphate Esters: Solvation versus Strain. *J. Am. Chem. Soc.* **115**, 12 (1993), 5316–5317.

(52) TOLE, P., AND LIM, C. New Insights into the Base-Catalyzed Hydrolysis of Methyl Ethylene Phosphate. *J. Phys. Chem.* **97** (1993), 6212–6219.

(53) TOLE, P., AND LIM, C. The Significance of Electrostatic Effects in Phospho-Ester Hydrolysis. *J. Am. Chem. Soc.* **116**, 9 (1994), 3922–3931.

(54) CHANG, N., AND LIM, C. An *ab initio* study of nucleophilic attack of trimethyl phosphate: Factors influencing site reactivity. *J. Phys. Chem. A* **101** (1997), 8706–8713.

(55) MERCERO, J. M., BARRETT, P., LAM, C. W., FOWLER, J. E., UGALDE, J. M., AND PEDERSEN, L. G. Quantum Mechanical Calculations on Phosphate Hydrolysis Reactions. *J. Comput. Chem.* **21** (2000), 43–51.

(56) LOPEZ, X., DEJAEGERE, A., AND KARPLUS, M. Solvent Effects on the Reaction Coordinate of the Hydrolysis of Phosphates and Sulfates: Application of Hammond and Anti-Hammond Postulates to Understand Hydrolysis in Solution. *J. Am. Chem. Soc.* **123** (2001), 11755–11763.

(57) ÅQVIST, J., KOLMODIN, K., FLORIAN, J., AND WARSHEL, A. Mechanistic alternatives in phosphate monoester hydrolysis: what conclusions can be drawn from avaliable experimental data? *Chem. Biol.* **6**, 3 (1999), R71–R80.

(58) FLORIÁN, J., AND WARSHEL, A. A fundamental assumption about OH-attack in phosphate ester hydrolysis is not fully justified. *J. Am. Chem. Soc.* **119** (1997), 5473–5474.

(59) HU, C.-H., AND BRINCK, T. Theoretical Studies of the Hydrolysis of the Methyl Phosphate Anion. *J. Phys. Chem. A* **103** (1999), 5379–5386.

(60) WARSHEL, A., AND LEVITT, M. Theoretic studies of enzymatic reactions:dielectric electrostatic and steric stabilization in the reaction of lysozyme. *J. Mol. Biol.* **103** (1976), 227–249.

(61) WARSHEL, A. Computer simulations of enzyme catalysis: methods, progress, and insights. *Annu. Rev. Biophys. Biomol. Struct.* **32** (2003), 425–443.

(62) GARCIA-VILOCA, M., GAO, J., KARPLUS, M., AND TRUHLAR, D. G. How enzymes work: analysis by modern rate theory and computer simulations. *Science* **303** (2004), 186–195.

(63) GOEDECKER, S. Linear scaling electronic structure methods. *Rev. Mod. Phys.* **71** (1999), 1085–1123.

(64) GOGONEA, V., SUÁREZ, D., VAN DER VAART, A., AND MERZ, JR, K. M. New developments in applying quantum mechanics to proteins. *Curr. Opin. Struct. Biol.* **11** (2001), 217–223.

(65) THIEL, W. Perspectives on semiempirical molecular orbital theory. In *Adv. Chem. Phys.*, I. Prigogine and S. A. Rice, Eds., vol. 93. John Wiley and Sons, New York, 1996, pp. 703–757.

(66) CLARK, T. Quo vadis semiempirical MO-theory? *J. Mol. Struct. (Theochem)* **530** (2000), 1–10.

(67) LOPEZ, X., AND YORK, D. M. Parameterization of semiempirical methods to treat nucleophilic attacks to biological phosphates: AM1/d parameters for phosphorus. *Theor. Chem. Acc.* **109** (2003), 149–159.

(68) MÖHLE, K., HOFMANN, H., AND THIEL, W. Description of peptide and protein secondary sructures employing semiempirical methods. *J. Comput. Chem.* **22** (2001), 509–520.

(69) ELSTNER, M., FRAUENHEIM, T., KAXIRAS, E., SEIFERT, G., AND SUHAI, S. A Self-Consistent Charge Density-Functional Based Tight-Binding Scheme for Large Biomolecules. *Phys. Status Solidi. B* **217** (2000), 357–376.

(70) CUI, Q., ELSTNER, M., AND KARPLUS, M. A Theoretical Analysis of the Proton and Hydride Transfer in Liver Alcohol Dehydrogenase (LADH). *J. Phys. Chem. B* **106** (2002), 2721–2740.

(71) ELSTNER, M., CUI, Q., MUNIH, P., KAXIRAS, E., FRAUENHEIM, T., AND KARPLUS, M. Modeling zinc in biomolecules with the self consistent charge-density functional tight binding (SCC-DFTB) method: applications to structural and energetic analysis. *J. Comput. Chem.* **24** (2003), 565–581.

Table 1: Definition of phosphorane geometry and motion in pentavalent phosphorous pseudorotation reaction[1]

Molecule	Symbol	R	S	E	A	B
Fluorinated Model System						
P(**F**)(F)(F)(F)(F)	$P_F^{(V)}-\mathbf{1}$	**F**	F	F	F	F
Acyclic Phosphoranes						
P(**OH**)(OCH_3)(OCH_3)(OCH_3)(OCH_3)	$P_A^{(V)}-\mathbf{1}$	**OH**	OCH_3	OCH_3	OCH_3	OCH_3
P($\mathbf{O^-}$)(OCH_3)(OCH_3)(OCH_3)(OCH_3)	$P_A^{(V)}-\mathbf{1^-}$	$\mathbf{O^-}$	OCH_3	OCH_3	OCH_3	OCH_3
P(**OH**)(OH)(OCH_3)(OCH_3)(OCH_3)	$P_A^{(V)}-\mathbf{2a}$	**OH**	OH	OCH_3	OCH_3	OCH_3
P(**OH**)(OCH_3)(OCH_3)(OH)(OCH_3)	$P_A^{(V)}-\mathbf{2b}$	**OH**	OCH_3	OCH_3	OH	OCH_3
P($\mathbf{O^-}$)(OH)(OCH_3)(OCH_3)(OCH_3)	$P_A^{(V)}-\mathbf{2a^-}$	$\mathbf{O^-}$	OH	OCH_3	OCH_3	OCH_3
P($\mathbf{O^-}$)(OCH_3)(OCH_3)(OH)(OCH_3)	$P_A^{(V)}-\mathbf{2b^-}$	$\mathbf{O^-}$	OCH_3	OCH_3	OH	OCH_3
P(**OH**)(OH)(OCH_3)(OH)(OCH_3)	$P_A^{(V)}-\mathbf{3a}$	**OH**	OH	OCH_3	OH	OCH_3
P(**OH**)(OH)(OCH_3)(OH)(OCH_3)	$P_A^{(V)}-\mathbf{3b}$	**OH**	OH	OCH_3	OH	OCH_3
P($\mathbf{O^-}$)(OH)(OCH_3)(OH)(OCH_3)	$P_A^{(V)}-\mathbf{3a^-}$	$\mathbf{O^-}$	OH	OCH_3	OH	OCH_3
P($\mathbf{O^-}$)(OH)(OCH_3)(OH)(OCH_3)	$P_A^{(V)}-\mathbf{3b^-}$	$\mathbf{O^-}$	OH	OCH_3	OH	OCH_3
P(**OH**)(OH)(OH)(OH)(OCH_3)	$P_A^{(V)}-\mathbf{4a}$	**OH**	OH	OH	OH	OCH_3
P(**OH**)(OH)(OCH_3)(OH)(OH)	$P_A^{(V)}-\mathbf{4b}$	**OH**	OCH_3	OH	OH	OH
P($\mathbf{O^-}$)(OH)(OH)(OH)(OCH_3)	$P_A^{(V)}-\mathbf{4a^-}$	$\mathbf{O^-}$	OH	OH	OH	OCH_3
P($\mathbf{O^-}$)(OH)(OCH_3)(OH)(OH)	$P_A^{(V)}-\mathbf{4b^-}$	$\mathbf{O^-}$	OCH_3	OH	OH	OH
P(**OH**)(OH)(OH)(OH)(OH)	$P_A^{(V)}-\mathbf{5}$	**OH**	OH	OH	OH	OH
P($\mathbf{O^-}$)(OH)(OH)(OH)(OH)	$P_A^{(V)}-\mathbf{5^-}$	$\mathbf{O^-}$	OH	OH	OH	OH
Cyclic Phosphoranes						
P(**OH**)(OCH_3)(-O-CH_2CH_2-O-)(OCH_3)	$P_C^{(V)}-\mathbf{1a}$	**OH**	OCH_3	-O-CH_2CH_2-O-		OCH_3
P(**OH**)(OCH_3)(-O-CH_2CH_2-O-)(OCH_3)	$P_C^{(V)}-\mathbf{1b}$	**OH**	OCH_3	-O-CH_2CH_2-O-		OCH_3
P($\mathbf{O^-}$)(OCH_3)(-O-CH_2CH_2-O-)(OCH_3)	$P_C^{(V)}-\mathbf{1a^-}$	$\mathbf{O^-}$	OCH_3	-O-CH_2CH_2-O-		OCH_3
P($\mathbf{O^-}$)(OCH_3)(-O-CH_2CH_2-O-)(OCH_3)	$P_C^{(V)}-\mathbf{1b^-}$	$\mathbf{O^-}$	OCH_3	-O-CH_2CH_2-O-		OCH_3
P(**OH**)(OH)(-O-CH_2CH_2-O-)(OCH_3)	$P_C^{(V)}-\mathbf{2a}$	**OH**	OH	-O-CH_2CH_2-O-		OCH_3
P(**OH**)(OCH_3)(-O-CH_2CH_2-O-)(OH)	$P_C^{(V)}-\mathbf{2b}$	**OH**	OCH_3	-O-CH_2CH_2-O-		OH
P($\mathbf{O^-}$)(OH)(-O-CH_2CH_2-O-)(OCH_3)	$P_C^{(V)}-\mathbf{2a^-}$	$\mathbf{O^-}$	OH	-O-CH_2CH_2-O-		OCH_3
P($\mathbf{O^-}$)(OCH_3)(-O-CH_2CH_2-O-)(OH)	$P_C^{(V)}-\mathbf{2b^-}$	$\mathbf{O^-}$	OCH_3	-O-CH_2CH_2-O-		OH
P(**OH**)(OH)(-O-CH_2CH_2-O-)(OH)	$P_C^{(V)}-\mathbf{3}$	**OH**	OH	-O-CH_2CH_2-O-		OH
P($\mathbf{O^-}$)(OH)(-O-CH_2CH_2-O-)(OH)	$P_C^{(V)}-\mathbf{3^-}$	$\mathbf{O^-}$	OH	-O-CH_2CH_2-O-		OH

[1] The phosphorane ligands are generically labeled "A" and "B" in the axial positions, and "R", "S", and "E" in the equitorial positions (Scheme 1). For pseudorotation reactions, the pivotal ligand is indicated by boldface type. See text for additional discussion of the nomeclature convention adopted in this work.

Table 2: Average geometrical quantities for minimum energy structures of oxyphosphoranes[1]

	neutral				monoanionic			
Quantity	acyclic		cyclic		acyclic		cyclic	
Bond lengths								
P–O_{eq}(H)	1.638	(0.006)	1.633	(0.005)	1.671	(0.004)	1.662	(0.009)
P–O_{ax}(H)	1.689	(0.006)	1.681	(0.005)	1.778	(0.022)	1.726	(0.028)
P–O_{eq}(C)	1.630	(0.007)	1.646	(0.016)	1.684	(0.005)	1.693	(0.014)
P–O_{ax}(C)	1.710	(0.028)	1.749	(0.027)	1.779	(0.022)	1.827	(0.105)
P–O^-_{eq}	—	(—)	—	(—)	1.526	(0.007)	1.513	(0.005)
Bond Angles								
O_{ax}–P–O_{ax}	176.8	(1.6)	175.7	(3.0)	166.6	(3.0)	164.9	(2.6)
O_{ax}–P–O_{eq}	90.0	(1.8)	90.0	(2.1)	86.6	(2.3)	86.1	(2.9)
O_{eq}–P–O_{eq}	119.9	(3.1)	119.9	(3.8)	113.7	(2.5)	114.4	(2.7)
O_{ax}–P–O^-_{eq}	—	(—)	—	(—)	96.4	(1.6)	97.3	(3.6)
O_{eq}–P–O^-_{eq}	—	(—)	—	(—)	123.1	(2.9)	122.5	(3.4)

[1] Average bond lengths are in Å, and average bond angles are in degrees. Oxygen atoms bonded to phosphorus are classified into different types distinguished by their ligand positions, indicated as the subscripts ax (axial) and eq (equatorial), their connectivity with other atoms, indicated by parentheses around the atom covalently bonded to oxygen, and in the case of monoanionic phosphoranes, by formal charge O/O^-. Averages are calculated over neutral and monoanionic acyclic and cyclic phosphoranes, and root-mean-square deviations are given in parentheses.

Table 3: Geometrical quantities for pseudorotation transition state structures of oxyphosphoranes[1]

TS Structure	$< bl_{ax} >$	$< bl_{eq} >$	$\Delta < bl_{ax} >$	$\Delta < bl_{eq} >$	θ_1	θ_2	%SP
Fluorinated Model System							
$P_F^{(V)}-[\mathbf{1},\mathbf{1}]$	1.597	1.597	-0.009	0.023	155.1	155.1	100.0
Neutral Acyclic Phosphoranes							
$P_A^{(V)}-[\mathbf{1},\mathbf{1}]$	1.666	1.668	-0.029	0.038	155.6	155.0	99.0
$P_A^{(V)}-[\mathbf{2a},\mathbf{2b}]$	1.676	1.664	-0.026	0.030	155.0	155.3	99.6
$P_A^{(V)}-[\mathbf{3a},\mathbf{3b}]$	1.673	1.670	-0.030	0.037	154.0	155.6	97.3
$P_A^{(V)}-[\mathbf{4a},\mathbf{4b}]$	1.681	1.660	-0.020	0.025	156.8	152.1	92.2
$P_A^{(V)}-[\mathbf{5},\mathbf{5}]$	1.674	1.673	-0.028	0.038	154.0	154.6	99.0
Anionic Acyclic Phosphoranes							
$P_A^{(V)}-[\mathbf{1},\mathbf{1}]^-$	1.730	1.730	-0.035	0.043	143.1	143.1	100.0
$P_A^{(V)}-[\mathbf{2a},\mathbf{2b}]^-$	1.699	1.758	-0.087	0.082	123.0	159.9	38.5
$P_A^{(V)}-[\mathbf{3a},\mathbf{3b}]^-$	1.734	1.739	-0.047	0.064	140.9	144.8	93.5
$P_A^{(V)}-[\mathbf{4a},\mathbf{4b}]^-$	1.706	1.763	-0.085	0.094	128.0	155.9	53.5
$P_A^{(V)}-[\mathbf{5},\mathbf{5}]^-$	1.739	1.739	-0.045	0.070	142.6	142.6	100.0
Neutral Cyclic Phosphoranes							
$P_C^{(V)}-[\mathbf{1a},\mathbf{1b}]$	1.675	1.674	-0.024	0.034	155.5	155.2	99.6
$P_C^{(V)}-[\mathbf{2a},\mathbf{2b}]$	1.682	1.668	-0.019	0.027	156.7	153.4	94.5
$P_C^{(V)}-[\mathbf{3},\mathbf{3}]$	1.677	1.676	-0.023	0.033	154.7	155.0	99.6
Anionic Cyclic Phosphoranes							
$P_C^{(V)}-[\mathbf{1a},\mathbf{1b}]^-$	1.764	1.716	-0.014	0.019	152.5	132.5	66.6
$P_C^{(V)}-[\mathbf{2a},\mathbf{2b}]^-$	1.707	1.765	-0.137	0.092	124.0	159.5	40.9
$P_C^{(V)}-[\mathbf{3},\mathbf{3}]^-$	1.730	1.765	-0.124	0.096	145.8	139.3	89.2

[1] Each of the transition state structures listed above uniquely connects two of the minimum energy structures indicated in brackets. The designation of "axial" and "equitorial" have little meaning for the actual transition state structures themselves that have largely a square-pyramidal structure. Nonetheless, it is useful to distinguish those bonds in the transition state that correspond to the axial and equatorial bonds of the reactant, that by convention are defined as the lowest of the two energy minima connected by the transition state. The quantities $< bl_{ax} >$ and $< bl_{eq} >$ refer to the average bond lengths in the transition state that correspond to the axial and equatorial bonds being exchanged, respectively, of the reactant structure. The quantities $\Delta < bl_{ax} >$ and $\Delta < bl_{eq} >$ measure the *change* in the average axial and equatorial bond lengths that occur in going from reactant to transition state. All average bond length quantities are in Å. Also listed are the axial and equatorial O–P–O bond angles (θ_1 and θ_2, respectively) in degrees and the "square-pyramidal character" percentage (%SP) defined by the empirical formula $\%\mathrm{SP} = [1 - |\theta_1 - \theta_2|/60] \times 100$.

Table 4: Calculated thermodynamic data for gas-phase pseudorotation reactions of oxyphosphoranes[1]

	Net Reaction				Rate-limiting TS			
Reaction	ΔH	$-T\Delta S$	ΔG	Δn_{HB}	$\Delta H^{\ddagger}$	$-T\Delta S^{\ddagger}$	$\Delta G^{\ddagger}$	$\Delta n^{\ddagger}_{HB}$
Fluorinated model system								
$P_F^{(V)}$–[**1, 1**]	—	—	—	0	3.12	0.01	3.14	0
Neutral acyclic phosphoranes								
$P_A^{(V)}$–[**1, 1**]	—	—	—	0	6.50	0.52	7.02	-1
$P_A^{(V)}$–[**2a, 2b**]	3.04	-0.79	2.25	-1	7.45	0.62	8.07	-1
$P_A^{(V)}$–[**3a, 3b**]	0.21	-0.16	0.06	0	5.54	0.73	6.27	0
$P_A^{(V)}$–[**4a, 4b**]	0.46	-0.02	0.45	0	5.07	0.90	5.97	0
$P_A^{(V)}$–[**5, 5**]	—	—	—	0	5.24	0.91	6.24	0
Monoanionic acyclic phosphoranes								
$P_A^{(V)}$–[**1, 1**]$^-$	—	—	—	0	1.12	2.24	3.35	0
$P_A^{(V)}$–[**2a, 2b**]$^-$	5.74	-0.29	5.45	0	5.85	0.86	6.71	-1
$P_A^{(V)}$–[**3a, 3b**]$^-$	3.79	0.12	3.92	0	3.54	1.39	4.93	0
$P_A^{(V)}$–[**4a, 4b**]$^-$	4.71	-0.39	4.32	0	7.54	0.19	7.73	-2
$P_A^{(V)}$–[**5, 5**]$^-$	—	—	—	0	6.08	1.11	7.19	-4
Neutral cyclic phosphoranes								
$P_C^{(V)}$–[**1a, 1b**]	5.13	-0.45	4.67	0	6.86	0.77	7.62	-1
$P_C^{(V)}$–[**2a, 2b**]	4.15	-0.86	3.29	-1	6.82	0.62	7.23	-1
$P_C^{(V)}$–[**3, 3**]	—	—	—	0	4.48	0.90	5.38	0
Monoanionic cyclic phosphoranes								
$P_C^{(V)}$–[**1a, 1b**]$^-$	-0.05	0.14	0.08	0	0.43	1.06	1.49	0
$P_C^{(V)}$–[**2a, 2b**]$^-$	3.88	0.28	4.16	0	4.08	1.17	5.25	-1
$P_C^{(V)}$–[**3, 3**]$^-$	—	—	—	0	1.71	1.34	3.05	-1

[1] Values for the change free energy (ΔG) in the gas phase are listed along with the enthalpic (ΔH) and entropic ($-T\Delta S$) contributions, and change in the number of intramolecular equatorial↔axial hydrogens bonds (Δn_{HB}). Thermodynamic changes are with respect to reactants, defined as the lower free energy isomer, and correspond to a temperature T=298.15 K. All units are kcal/mol. The pseudorotation "reaction" is indicated by the abbreviation for the rate-limiting transition state that connects the reactant and product isomers. The change in thermodynamic quantities for the net reaction are shown without superscript, and the corresponding change in thermodynamic quantities for the rate-limiting transition state are superscripted by a double-dagger (‡).

Table 5: Calculated change in solvation free energy for pseudorotation reactions of oxyphosphoranes[1]

	$\Delta\Delta G_{sol}$ - Net Reaction			$\Delta\Delta G^{\ddagger}_{sol}$ - Rate-limiting TS		
Reaction	PCM	COSMO	SM5	PCM	COSMO	SM5
Fluorinated model system						
$P_F^{(V)}-[\mathbf{1,1}]$	—	—	—	-0.03	-0.04	0.08
Neutral acyclic phosphoranes						
$P_A^{(V)}-[\mathbf{1,1}]$	—	—	—	-1.01	-0.78	-0.71
$P_A^{(V)}-[\mathbf{2a,2b}]$	-1.24	-0.74	-0.07	-0.87	-1.01	-0.50
$P_A^{(V)}-[\mathbf{3a,3b}]$	-0.57	-0.23	0.29	-0.50	-0.48	-0.25
$P_A^{(V)}-[\mathbf{4a,4b}]$	0.73	1.14	-0.07	-0.16	0.31	-0.52
$P_A^{(V)}-[\mathbf{5,5}]$	—	—	—	-0.62	-0.47	-0.39
Monoanionic acyclic phosphoranes						
$P_A^{(V)}-[\mathbf{1,1}]^-$	—	—	—	0.64	0.51	0.05
$P_A^{(V)}-[\mathbf{2a,2b}]^-$	-1.48	-1.24	-0.91	-2.36	-2.28	-1.44
$P_A^{(V)}-[\mathbf{3a,3b}]^-$	-2.25	-2.29	-0.91	-1.05	-1.19	-0.80
$P_A^{(V)}-[\mathbf{4a,4b}]^-$	-0.97	-0.97	-0.81	-3.82	-3.84	-2.07
$P_A^{(V)}-[\mathbf{5,5}]^-$	—	—	—	-3.75	-3.66	-1.54
Neutral cyclic phosphoranes						
$P_C^{(V)}-[\mathbf{1a,1b}]$	-2.08	-2.58	-1.31	-1.62	-1.51	-0.94
$P_C^{(V)}-[\mathbf{2a,2b}]$	-1.11	-1.23	-0.69	-0.96	-0.83	-0.91
$P_C^{(V)}-[\mathbf{3,3}]$	—	—	—	-0.35	-0.26	-0.66
Monoanionic cyclic phosphoranes						
$P_C^{(V)}-[\mathbf{1a,1b}]^-$	-0.52	-0.40	0.15	0.74	0.68	0.19
$P_C^{(V)}-[\mathbf{2a,2b}]^-$	-2.45	-2.16	-1.79	-2.61	-2.50	-2.25
$P_C^{(V)}-[\mathbf{3,3}]^-$	—	—	—	-1.45	-1.41	-1.52

[1] Values for the change in solvation free energy ($\Delta\Delta G_{sol}$) are listed for three different solvation methods: PCM, COSMO and SM5 (see text). All values correspond to a temperature T=298.15 K. All units are kcal/mol. The pseudorotation "reaction" is indicated by the abbreviation for the rate-limiting transition state that connects the reactant and product isomers. The change in solvation free energy for the net reaction are shown without superscript, and the corresponding change in solvation free energy for the rate-limiting transition state are superscripted by a double-dagger (‡).

Table 6: Calculated change in aqueous-phase free energy for pseudorotation reactions of oxyphosphoranes[1]

	ΔG_{aq} - Net Reaction			$\Delta G^{\ddagger}_{aq}$ - Rate-limiting TS		
Reaction	PCM	COSMO	SM5	PCM	COSMO	SM5
Fluorinated model system						
$P_F^{(V)}-[\mathbf{1},\mathbf{1}]$	—	—	—	3.11	3.10	3.22
Neutral acyclic phosphoranes						
$P_A^{(V)}-[\mathbf{1},\mathbf{1}]$	—	—	—	6.01	6.24	6.31
$P_A^{(V)}-[\mathbf{2a},\mathbf{2b}]$	1.01	1.51	2.19	7.20	7.06	7.57
$P_A^{(V)}-[\mathbf{3a},\mathbf{3b}]$	-0.51	-0.17	0.35	5.77	5.79	6.02
$P_A^{(V)}-[\mathbf{4a},\mathbf{4b}]$	1.18	1.59	0.38	5.81	6.28	5.45
$P_A^{(V)}-[\mathbf{5},\mathbf{5}]$	—	—	—	5.53	5.68	5.76
Monoanionic acyclic phosphoranes						
$P_A^{(V)}-[\mathbf{1},\mathbf{1}]^-$	—	—	—	3.99	3.86	3.41
$P_A^{(V)}-[\mathbf{2a},\mathbf{2b}]^-$	3.97	4.21	4.54	4.35	4.43	5.26
$P_A^{(V)}-[\mathbf{3a},\mathbf{3b}]^-$	1.67	1.63	3.01	3.88	3.74	4.13
$P_A^{(V)}-[\mathbf{4a},\mathbf{4b}]^-$	3.35	3.35	3.51	3.91	3.89	5.66
$P_A^{(V)}-[\mathbf{5},\mathbf{5}]^-$	—	—	—	3.44	3.53	5.65
Neutral cyclic phosphoranes						
$P_C^{(V)}-[\mathbf{1a},\mathbf{1b}]$	2.59	2.09	3.36	6.00	6.11	6.68
$P_C^{(V)}-[\mathbf{2a},\mathbf{2b}]$	2.18	2.06	2.59	6.27	6.40	6.32
$P_C^{(V)}-[\mathbf{3},\mathbf{3}]$	—	—	—	5.03	5.12	4.72
Monoanionic cyclic phosphoranes						
$P_C^{(V)}-[\mathbf{1a},\mathbf{1b}]^-$	-0.44	-0.32	0.23	2.23	2.17	1.69
$P_C^{(V)}-[\mathbf{2a},\mathbf{2b}]^-$	1.71	2.00	2.37	2.64	2.75	3.00
$P_C^{(V)}-[\mathbf{3},\mathbf{3}]^-$	—	—	—	1.60	1.64	1.53

[1] Values for the change in aqueous-phase free energy (ΔG_{aq}) are listed for three different solvation methods: PCM, COSMO and SM5 (see text). All values correspond to a temperature T=298.15 K. All units are kcal/mol. The pseudorotation "reaction" is indicated by the abbreviation for the rate-limiting transition state that connects the reactant and product isomers. The change in aqueous-phase free energy for the net reaction are shown without superscript, and the corresponding change in aqueous-phase free energy for the rate-limiting transition state are superscripted by a double-dagger (‡).

Table 7: Comparison of calculated density-functional and semiempirical gas-phase enthalpies for pseudorotation reactions of oxyphosphoranes[1]

	ΔH - Net Reaction					$\Delta H^{\ddagger}$ - Rate-limiting TS				
Reaction	DFT	MNDO	AM1	PM3	MNDO/d	DFT	MNDO	AM1	PM3	MNDO/d
Fluorinated model system										
$P_F^{(V)}-[\mathbf{1,1}]$	—	—	—	—	—	3.12	3.81	2.77	4.10	3.57
Neutral acyclic phosphoranes										
$P_A^{(V)}-[\mathbf{1,1}]$	—	—	—	—	—	6.50	4.71	5.36	7.59	5.58
$P_A^{(V)}-[\mathbf{2a,2b}]$	3.04	-0.63	-1.33	-2.05	1.07	7.45	2.79	4.74	—	5.03
$P_A^{(V)}-[\mathbf{3a,3b}]$	0.21	-1.34	-0.92	-2.70	-0.09	5.54	2.59	3.50	—	5.12
$P_A^{(V)}-[\mathbf{4a,4b}]$	0.46	1.66	-0.06	1.69	2.06	5.07	4.55	1.94	2.06	—
$P_A^{(V)}-[\mathbf{5,5}]$	—	—	—	—	—	5.24	3.25	2.58	0.67	3.92
Monoanionic acyclic phosphoranes										
$P_A^{(V)}-[\mathbf{1,1}]^-$	—	—	—	—	—	1.12	2.54	—	—	3.81
$P_A^{(V)}-[\mathbf{2a,2b}]^-$	5.74	5.48	—	0.02	3.44	5.85	5.75	—	—	4.10
$P_A^{(V)}-[\mathbf{3a,3b}]^-$	3.79	1.04	1.33	-0.21	0.55	3.54	3.31	1.15	—	2.14
$P_A^{(V)}-[\mathbf{4a,4b}]^-$	4.71	2.36	—	-0.81	4.47	7.54	3.18	4.29	—	4.68
$P_A^{(V)}-[\mathbf{5,5}]^-$	—	—	—	—	—	6.08	1.16	0.08	—	1.61
Neutral cyclic phosphoranes										
$P_C^{(V)}-[\mathbf{1a,1b}]$	5.13	2.73	3.85	-1.68	0.11	6.86	1.64	5.72	3.06	3.41
$P_C^{(V)}-[\mathbf{2a,2b}]$	4.15	0.47	1.65	-0.02	1.08	6.82	3.03	4.34	3.00	4.77
$P_C^{(V)}-[\mathbf{3,3}]$	—	—	—	—	—	4.48	2.27	3.42	1.85	4.08
Monoanionic cyclic phosphoranes										
$P_C^{(V)}-[\mathbf{1a,1b}]^-$	-0.05	0.00	0.00	0.00	0.06	0.43	1.26	—	—	1.45
$P_C^{(V)}-[\mathbf{2a,2b}]^-$	3.88	1.35	—	—	3.34	4.08	1.59	3.44	4.16	3.47
$P_C^{(V)}-[\mathbf{3,3}]^-$	—	—	—	—	—	1.71	1.19	—	—	0.56

[1] Values for the change in enthalpy (ΔH) are listed for four different semiempirical methods: MNDO, AM1, PM3 and MNDO/d (see text). All values correspond to a temperature T=298.15 K. All units are kcal/mol. The pseudorotation "reaction" is indicated by the abbreviation for the rate-limiting transition state that connects the reactant and product isomers. The change in enthalpy for the net reaction are shown without superscript, and the corresponding change in enthalpy for the rate-limiting transition state are superscripted by a double-dagger (‡).

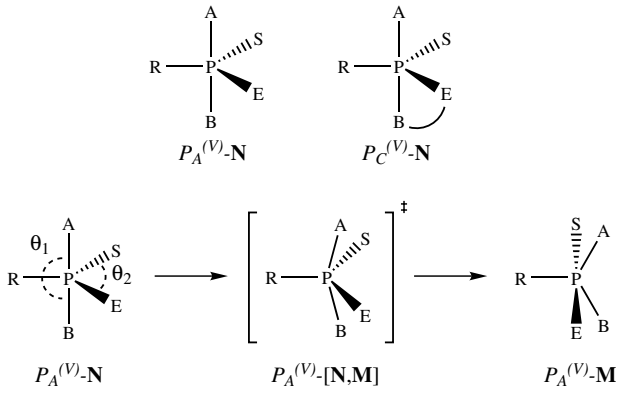

Scheme 1: Abbreviated nomenclature and structural notation for stationary points of pseudorotation reactions involving acyclic and cyclic phosphoranes. The pseudorotation reactants and products are trigonal bipyramidal structures, and the transition states (indicated by brackets) are square pyramidal structures. Acyclic and cyclic phosphoranes are indicated by subscripts "A" and "C", respectively. The **N** and **M** stand for the alpha-numeric index associated with one of the particular trigonal bipyramidal phosphorane listed in Table 1. A transition state that connects two minima is indicated by a set of brackets with both minima separated by a comma.

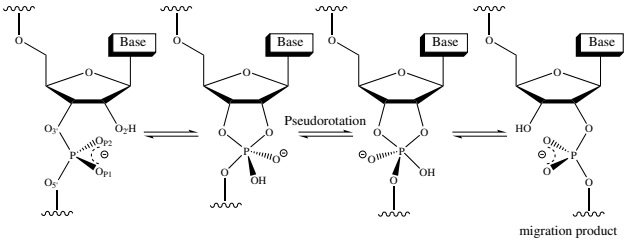

Scheme 2: Role of pseudorotation in the process of RNA phosphate migration.

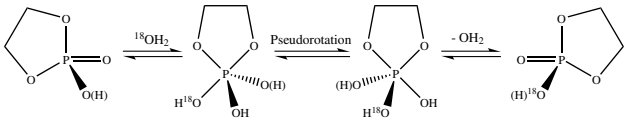

Scheme 3: Incorporation of ^{18}O in ethylene phosphate under non-alkaline conditions via a mechanism that involves pseudorotation.

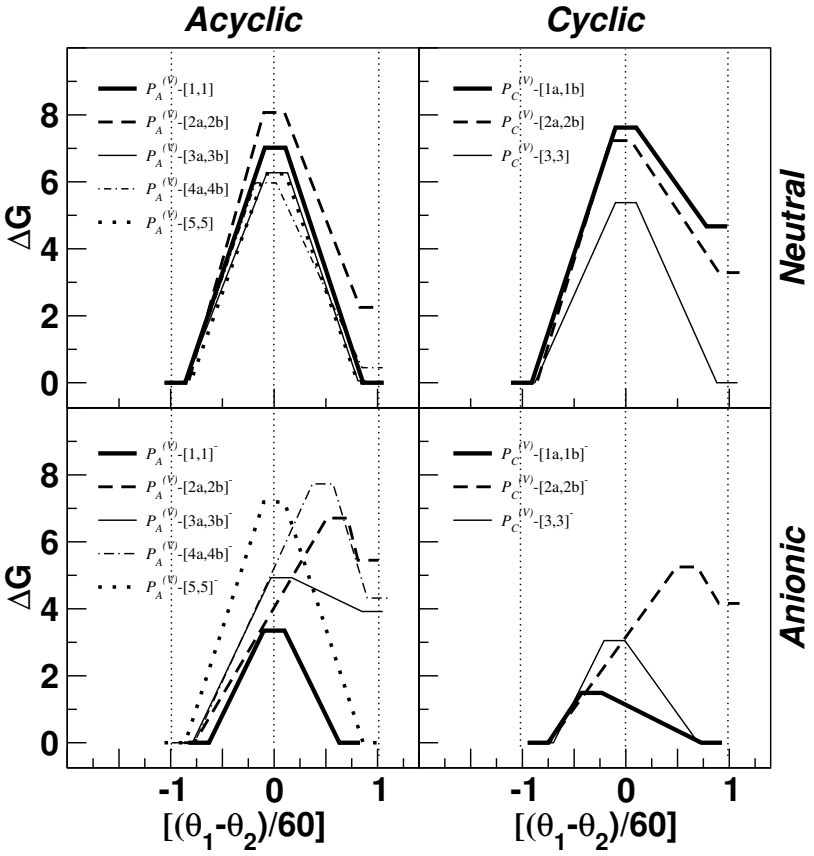

Figure 1: Reaction diagrams for pseudorotation of cyclic and acyclic oxyphosphoranes. Shown are neutral (top)/anionic (bottom) species, and acyclic (left)/cyclic (right) species. The lines are labeled with the convention proposed in Section 3.1 and summarized in Table 1. Dotted vertical lines at reaction coordinate values ($q = (\theta_1 - \theta_2)/60$) of 0 and ± 1 correspond to ideal square pyramidal transition state structures and trigonal bipyramidal reactant and product structures, respectively.

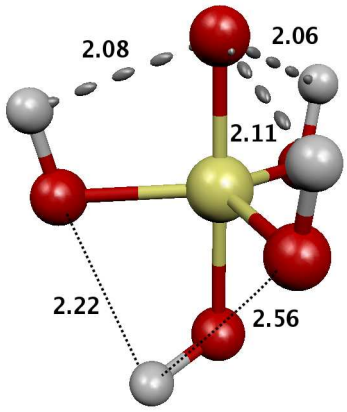

Figure 2: High-energy structure of phosphorane with anionic oxo group in the axial position.

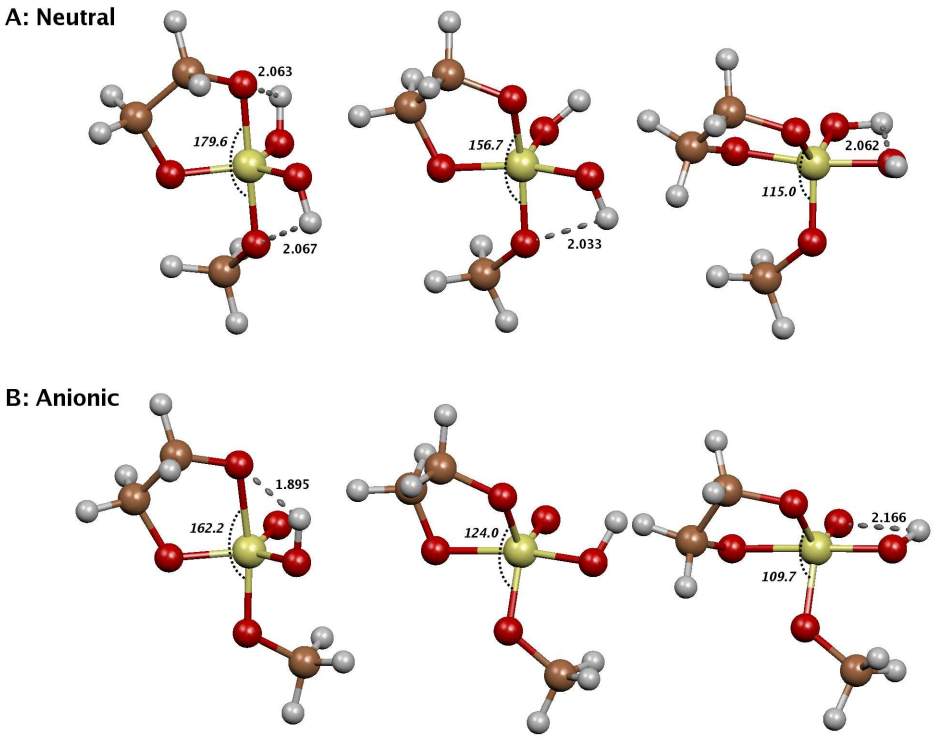

Figure 3: Pseudorotation diagram of methyl ethylene phosphorane, an intermediate in the hydrolysis of methyl ethylene phosphate: **A**) neutral state under acidic conditions, **B**) monoanionic state under neutral conditions.